Electronic Supplementary Information for:

# Commodity Elastomer-Derived Ordered Mesoporous Hard Carbon for High-Performance Sodium-Ion Battery Anodes

Anthony Griffin,[a,†] Hao Nguyen,[b,†] Jeff Aguinaga[a], Derek L. Patton[a], Zhe Qiang[a,*], and Shuya Wei[b,*]

[a]School of Polymer Science and Engineering, The University of Southern Mississippi, Hattiesburg, MS 39406, USA

[b]Department of Chemical and Biological Engineering, The University of New Mexico, Albuquerque, NM 87131, USA

[†]co-first authors

Corresponding authors: Z. Q. (zhe.qiang@usm.edu), S. W. (swei@unm.edu)

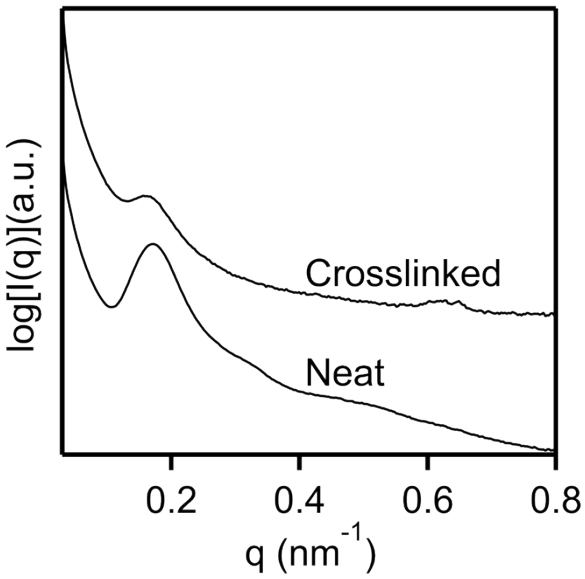


Figure S1. SAXS profiles for neat and crosslinked SEBS at at 145 °C for 75 min.

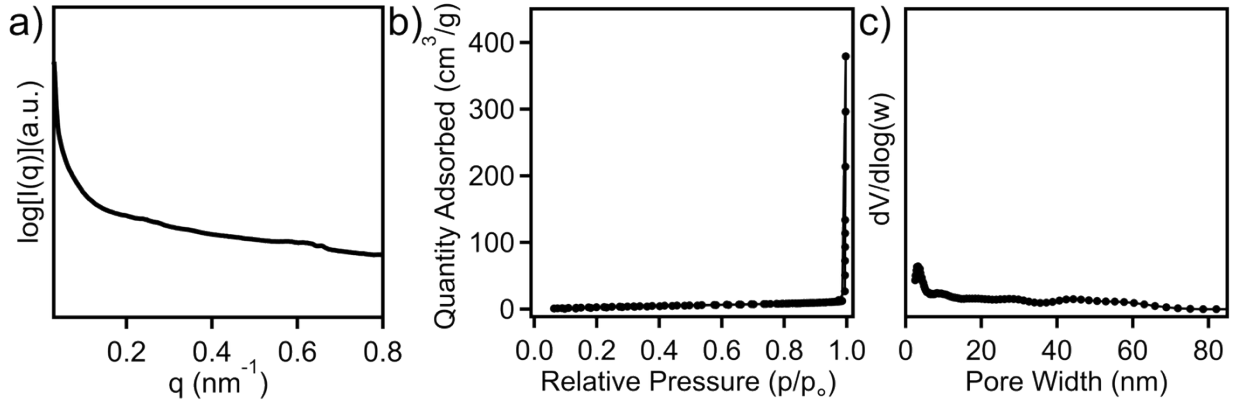


Figure S2. (a) SAXS profile, (b) nitrogen sorption isotherm, and (c) pore size distribution for a disordered carbon.

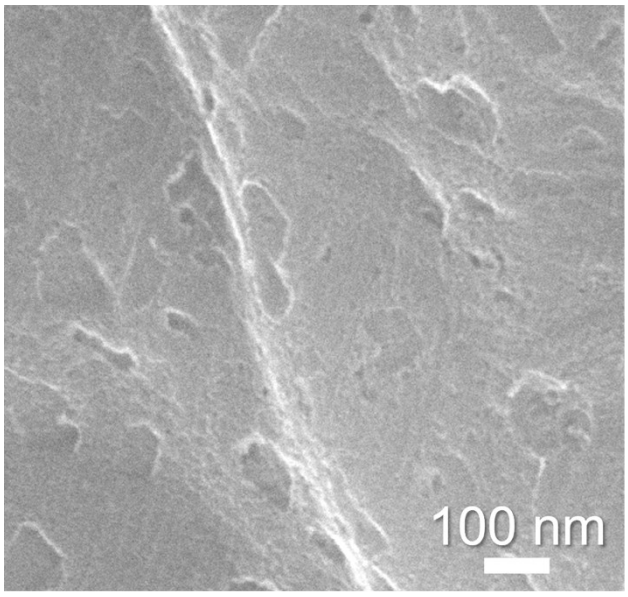


Figure S3. SEM micrograph of the disordered carbon prepared by pyrolysis of under-crosslinked SBS.

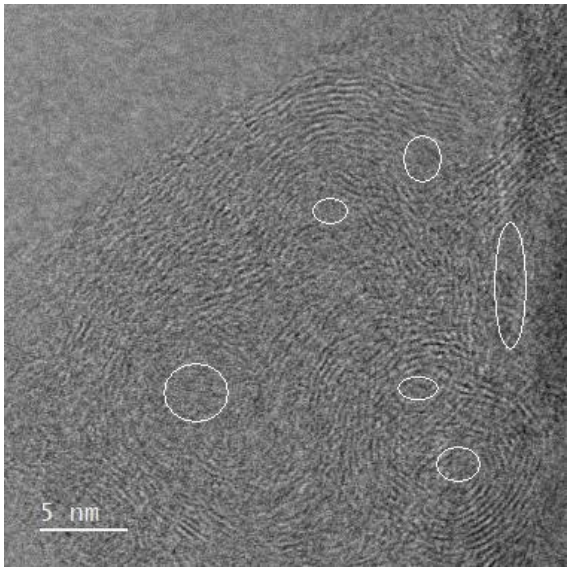


Figure S4. TEM image of OMHC-1300°C with closed-pore structures.

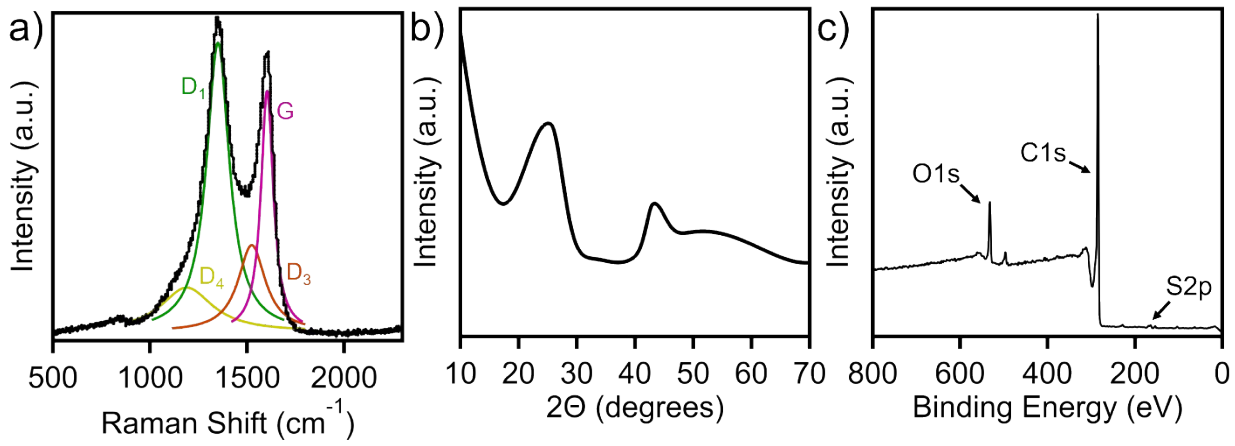


Figure S5. (a) Raman spectra, (b) representative XRD pattern, and (c) XPS survey scan for the disordered carbon prepared by pyrolysis of under-crosslinked SBS.

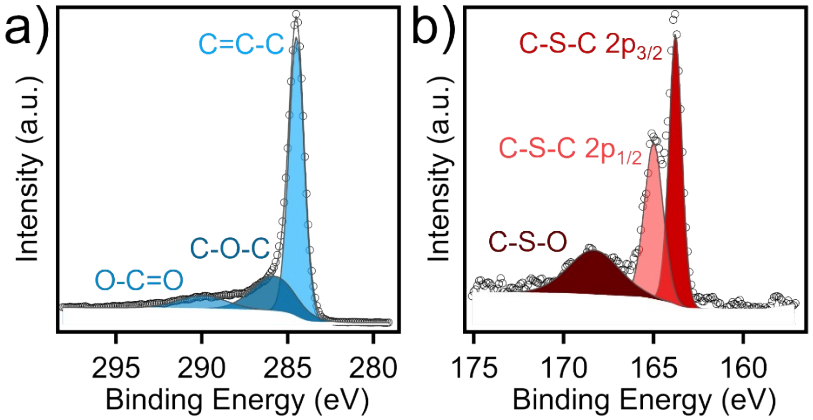


Figure S6. High-resolution XPS scans depicting (a) carbon and (b) sulfur bonding environments for a TPE-derived OMHC carbonized at 800 °C.

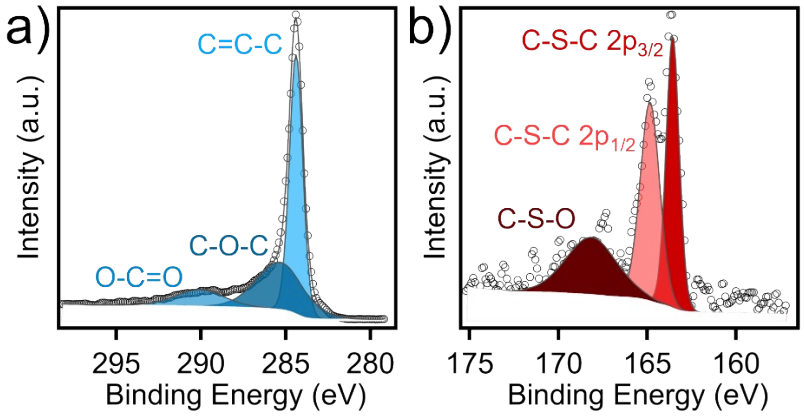


Figure S7. High-resolution XPS scans depicting (a) carbon and (b) sulfur bonding environments for a TPE-derived OMHC carbonized at 1,100 °C.

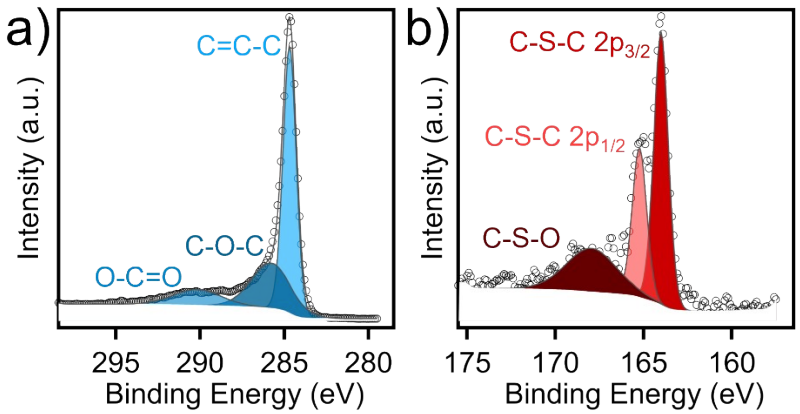


Figure S8. High-resolution XPS scans depicting (a) carbon and (b) sulfur bonding environments for a TPE-derived OMHC carbonized at 1,300 °C.

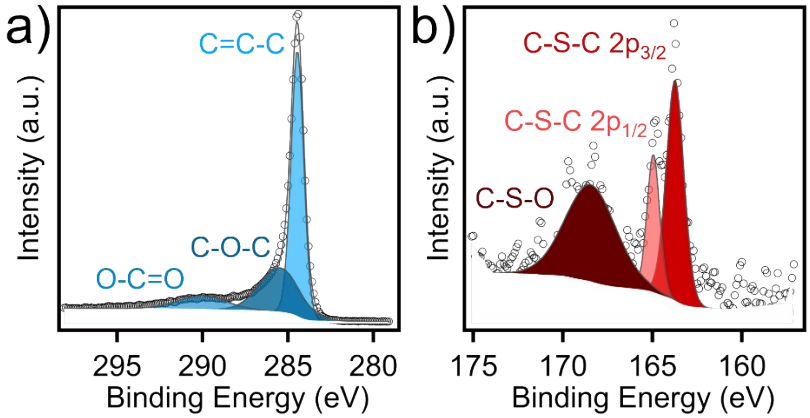


Figure S9. High-resolution XPS scans depicting (a) carbon and (b) sulfur bonding environments for a disordered carbon prepared by pyrolysis of under-crosslinked SBS.

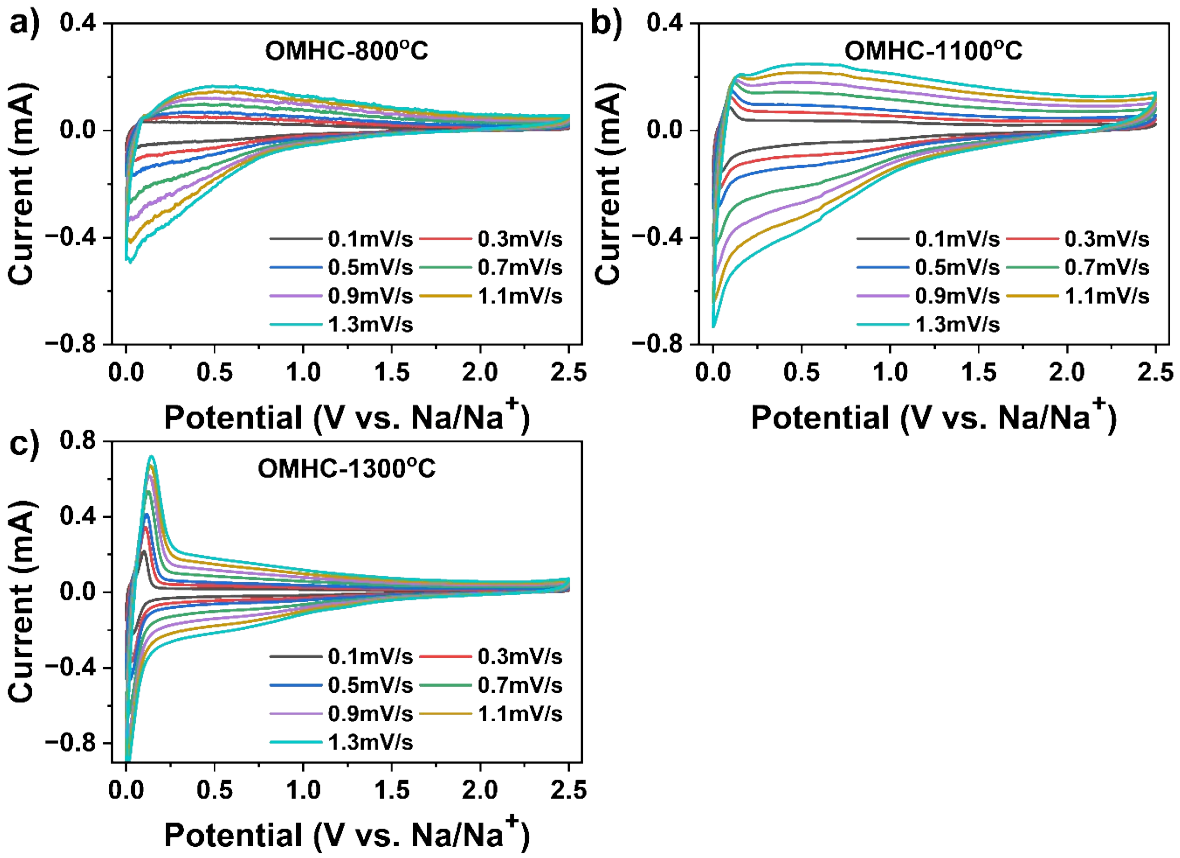


Figure S10. CV of a) OMHC-800 °C, b) OMHC-1100 °C and c) OMHC-1300 °C at various scan rates.

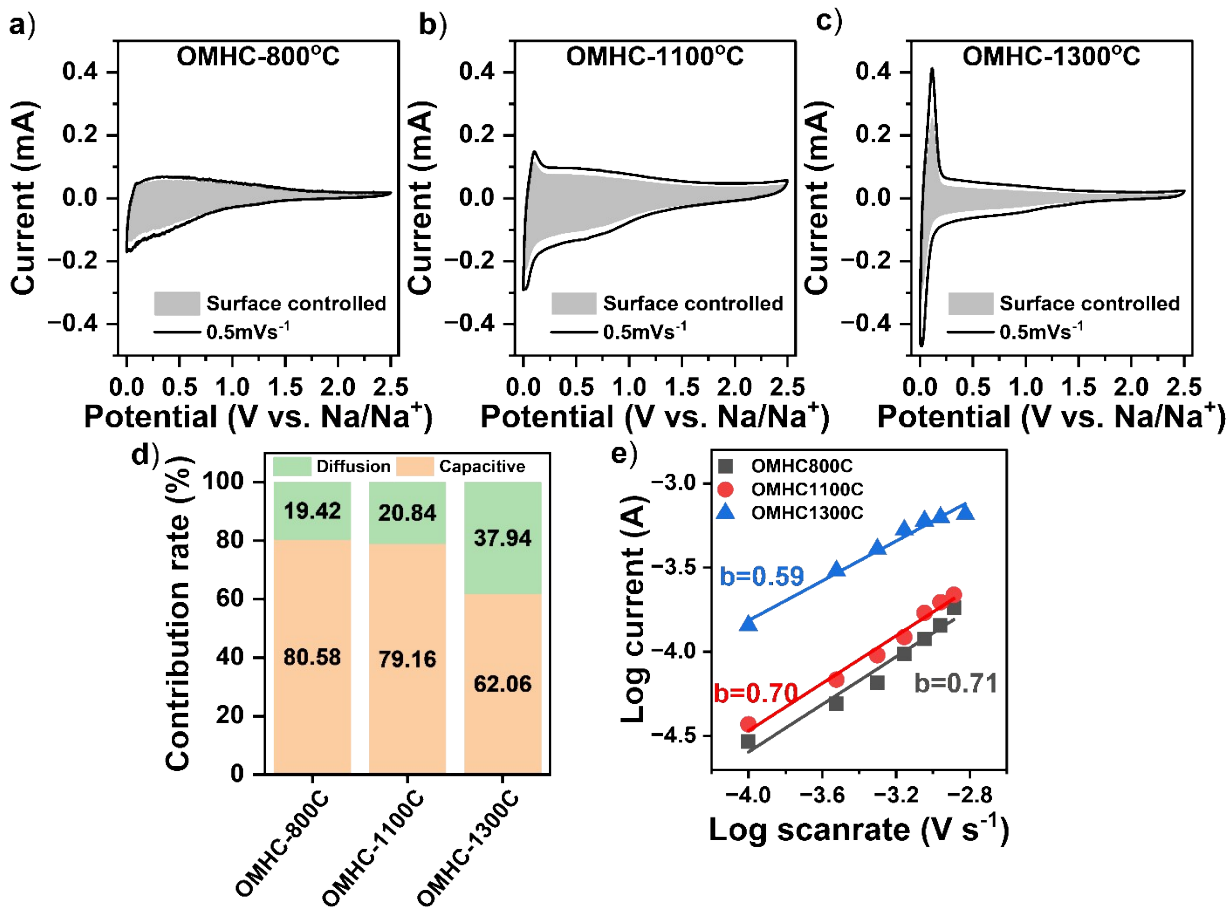


Figure S11. The visualization of the results after Dunn's analysis for a) OMHC-800 °C, b) OMHC-1100 °C and c) OMHC-1300 °C at 0.5 mV $s^{-1}$. d) Comparison of diffusion controlled and capacitive controlled of HC samples at 0.5mV $s^{-1}$. e) b-value determination of HC samples.

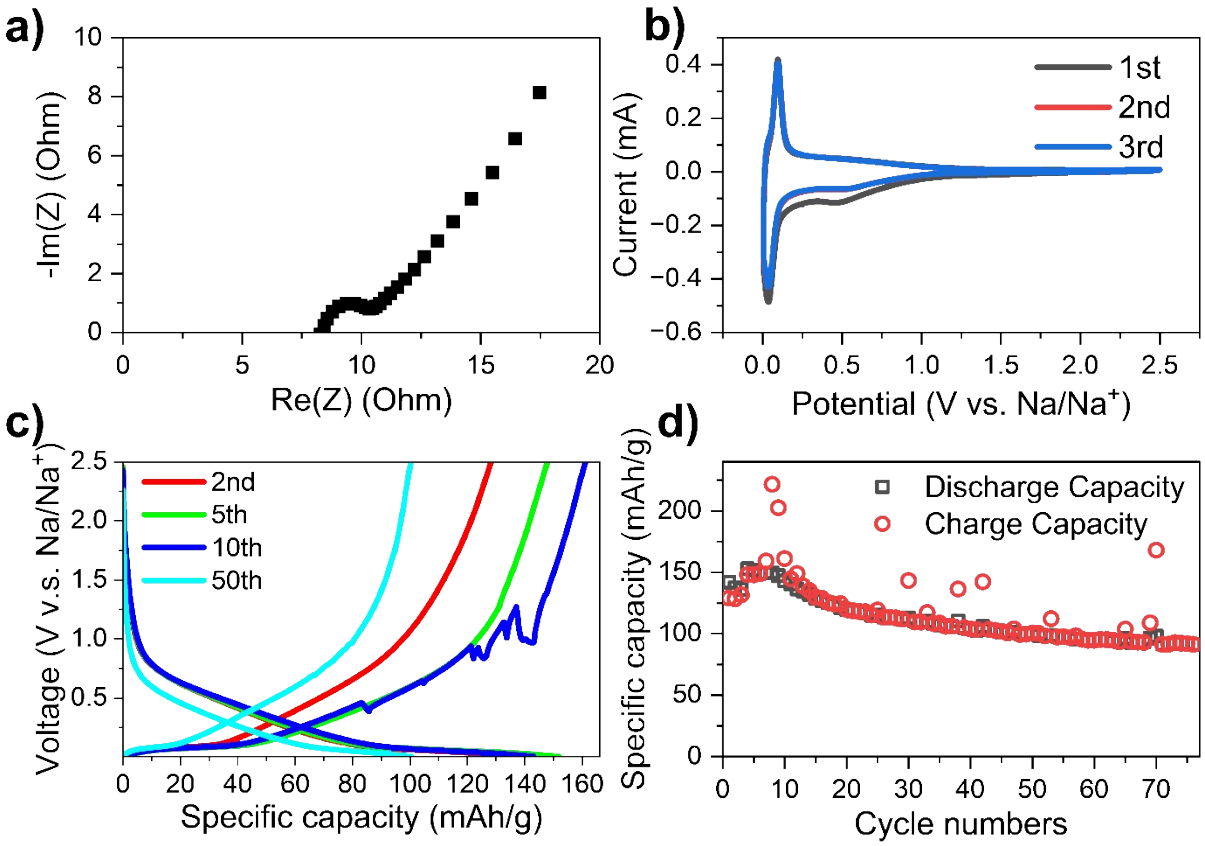


Figure S12. a) EIS, b) CV, c) GCD profile and d) GCD of the disordered carbon.

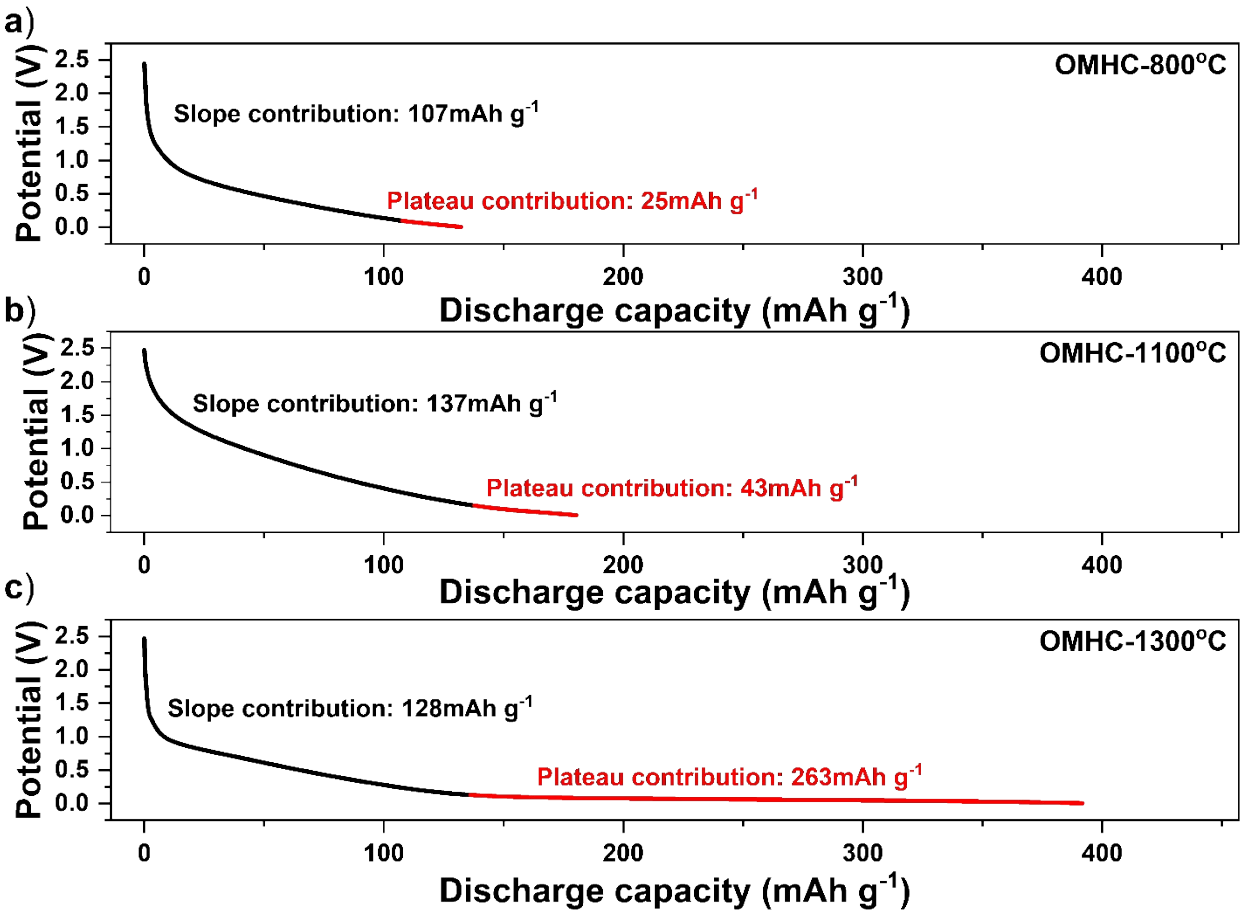


Figure S13. Split voltage profile of a) OMHC-800 °C, b) OMHC-1100 °C and c) OMHC-1300 °C into slope region (potential > 0.1V) and plateau region (potential < 0.1V) capacity contribution.

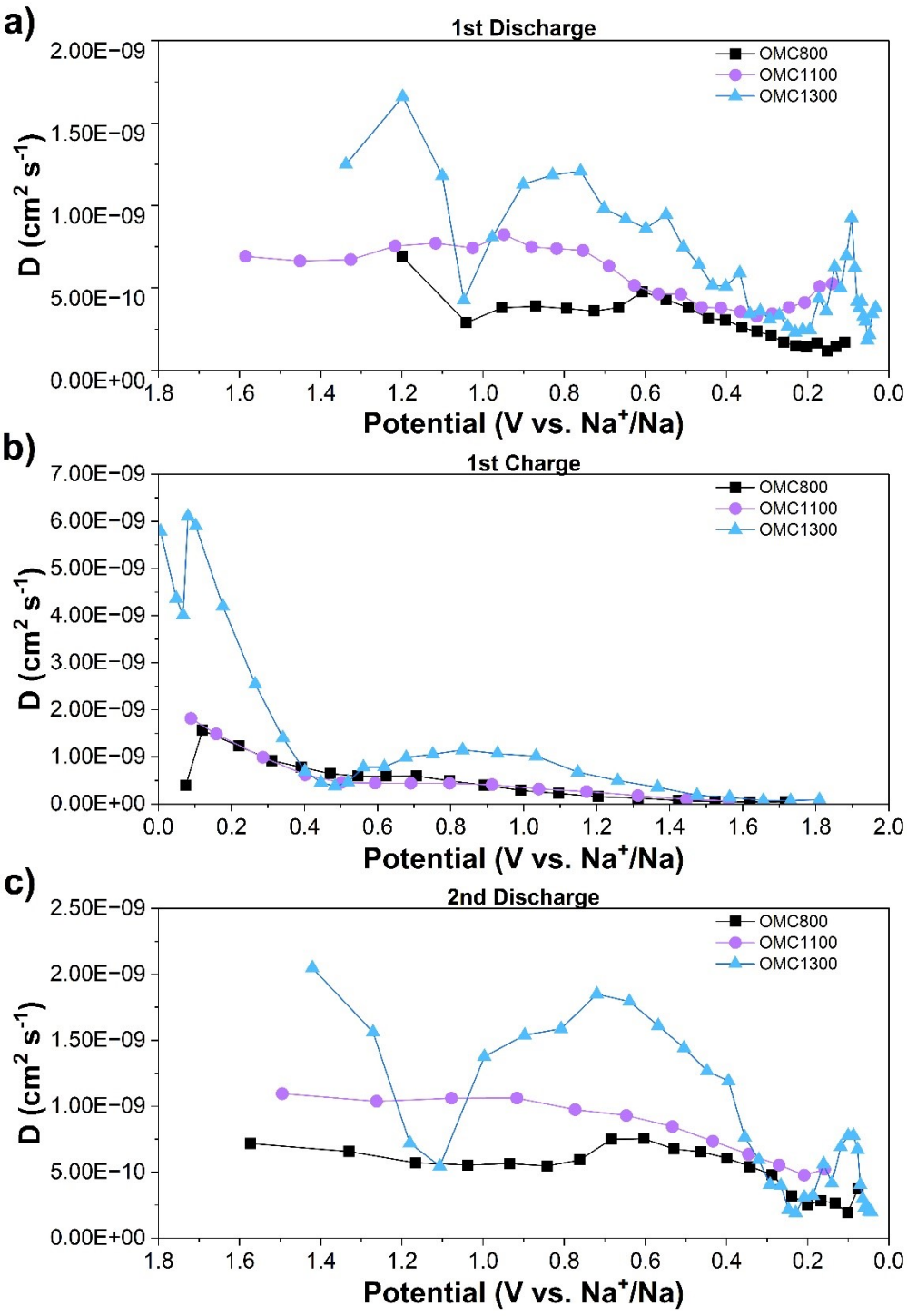


Figure S14. $D_{Na^+}$ values of hard carbon samples OMHC 800 °C, OMHC 1100°C, and OMHC 1300 °C by GITT measurements for a) 1st sodiation, b) 1st desodiation, and c) 2nd sodiation.

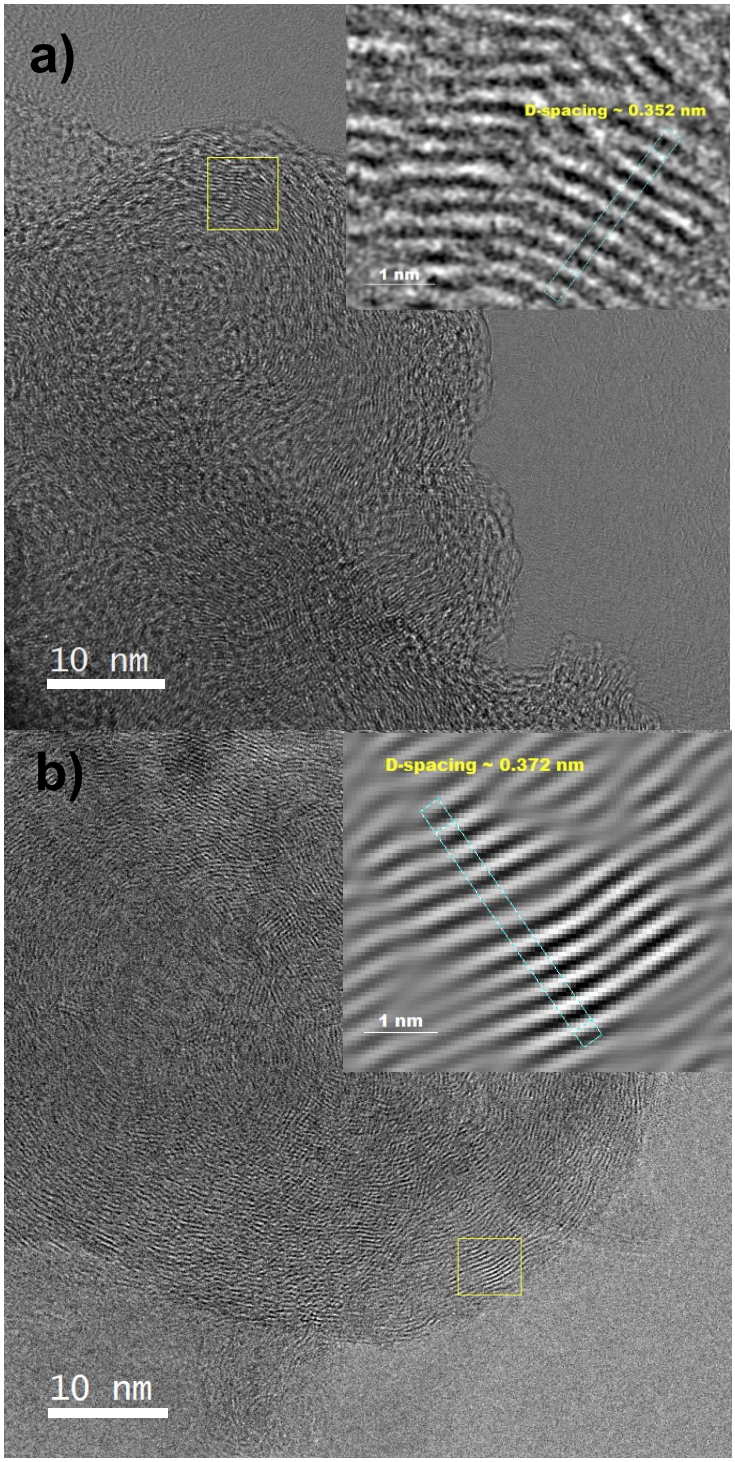


Figure S15. a) TEM of pristine OMHC-1300 °C with inset of d-spacing calculation and b) STEM of OMHC-1300 °C with inset of d-spacing calculation after 5 cycles of sodiation/desodiation.

Table S1. Structural parameters determined from XRD for all carbon anode materials used in this study

| Sample | $d_{002}$ (Å) | $L_c$ (nm) | $L_a$ (nm) |
|---|---|---|---|
| OMHC-800 °C | 3.79 | 0.59 | 7.2 |
| OMHC-1100 °C | 3.80 | 0.63 | 5.0 |
| OMHC-1300 °C | 3.66 | 0.91 | 3.9 |
| Disordered carbon | 3.62 | 0.96 | 6.4 |

Table S2. Elemental composition of all carbon anode materials used in this study, determined from XPS survey scans.

| | Elemental composition (at%) | | |
|---|---|---|---|
| Sample | Carbon | Oxygen | Sulfur |
| OMHC-800 °C | 92.3 | 6.3 | 1.4 |
| OMHC-1100 °C | 93.6 | 5.3 | 1.1 |
| OMHC-1300 °C | 94.6 | 4.4 | 1.0 |
| Disordered carbon | 93.2 | 6.1 | 0.7 |

Table S3. Relative ratios of carbon and sulfur peak intensities for all carbon anode materials used in this study, determined from high-resolution XPS scans.

| | Carbon (at%) | | | Sulfur (at%) | | |
|---|---|---|---|---|---|---|
| Sample | O-C=O | C-O-C | C=C-C | C-S-C $2p_{3/2}$ | C-S-C $2p_{1/2}$ | C-S-O |
| OMHC-800 °C | 10 | 24 | 66 | 41 | 33 | 26 |
| OMHC-1100 °C | 12 | 34 | 53 | 37 | 38 | 25 |
| OMHC-1300 °C | 13 | 29 | 58 | 48 | 26 | 26 |
| Disordered carbon | 11 | 31 | 58 | 37 | 17 | 47 |

Table S4. State of the art sodium hard carbon battery performance and this work.

| Classification | Precursor | Carbonization condition | Electrolyte | Cathode composition | Active material loading ($mg/cm^2$) | Potential window | Applied current | Initial capacity (mAh/g) | Reversible capacity (mAh/g) | ICE (%) | Cycles/ Retention rate |
|---|---|---|---|---|---|---|---|---|---|---|---|
| Biological waste | Rubber wood (2019)[1] | 350 °C for 1h then 900 °C for 1h in Ar | 1M $NaClO_4$ EC:DEC (1:1) | HC:SP:CMC:SBR (7:1.5:1:0.5) on Cu foil | 1.8-2.0 | 0.001-2.0V | 100 mA/g<br>5 A/g<br>10 A/g<br>15 A/g | 423<br>-<br>-<br>- | 275<br>85<br>66<br>45 | 56<br>-<br>-<br>- | 500/70%<br>250/-<br>250/-<br>4500/- |
| | Waste tea (2020)[2] | 1400 °C for 2h in Ar | 1M $NaClO_4$ EC:DEC (1:1) | HC:SP:PVDF (8:1:1) on Cu foil | 1.0 | 0-2.5V | 60 mA/g | 410 | 223.3 | 69 | 200/83% |
| | Corn stalk (2021)[3] | 800 °C for 1h in Ar | 1M $NaClO_4$ EC:DEC (1:1) | HC:AB:PVDF (8:1:1) on Cu foil | - | 0.01-2.8V | 100 mA/g | 2019 | 400 | 21 | 500/- |
| | Bagasse (2021)[4] | 1000 °C for 2h in Ar | 1M $NaPF_6$ EC:DEC (1:1) + 5wt% FEC | HC:SP:PVDF (8:1:1) on Al foil | 1.5-2.0 | 0.02-2.0V | 25 mA/g<br>1 A/g | 331.3<br>- | 242.1<br>- | 73.1<br>- | -<br>800/91.5% |
| | Lignen (2022)[5] | 1600 °C for 2h in Ar | 1M $NaPF_6$ DEGDME | HC:AB:PVDF (8:1:1) on Cu foil | - | 0-3.0V | 100 mA/g<br>500 mA/g | 373<br>258 | 303<br>163.4 | 75<br>63.29 | 200/-<br>200/- |
| | Camillia shell and coal-tar pitch (2025)[6] | 400 °C for 3h then 1400 °C for 3h in Ar | 1M NaPF6 EC:DEC (1:1) | HC:SP:CMC (9.4:0.4:0.2) on Cu foil | 1.0-1.2 | 0-2.0V | 20 mAh/g<br>50 mAh/g<br>200 mA/g<br>0.5 A/g | 385<br>-<br>-<br>- | 328<br>330<br>170<br>- | 86<br>-<br>- | -<br>-<br>1000/97.9%<br>2000/75.7% |
| Animal and plant organs | Lotus Seedpods (2019)[7] | 1200 °C for 2h in Ar | 1M $NaClO_4$ in PC + 2wt% FEC | HC:SP:PVDF (8:1:1) on Cu foil | - | 0.01-2.5 | 50 mA/g<br>200 mA/g | -<br>- | 328.8<br>201.8 | 50.4<br>- | 200/89.7%<br>500/80% |
| | Eggshell (2021)[8] | 1600 °C for 2h in Ar | 1M $NaClO_4$ in PC:EC (1:1) +5wt% FEC | HC:CB:CMC (8:1:1) on Cu foil | 1.5-2.0 | 0.01-3V | 30 mA/g | 412.2 | 329.8 | 80 | 100/73% |
| | Lotus Leaves (2021)[9] | 800 °C for 2h in Ar | 1M $NaClO_4$ in PC:EC (1:1) | HC:SP:PVDF (8:1:1) on Al foil | 2.5 ± 0.77 | 0.01-2.5V | 40 mA/g | 378 | 250 | 66 | 100/- |
| Biological extracts | Sucrose (2018)[10] | 1300 °C for 2h in Ar | 1M $NaClO_4$ EC:DEC (1:1) | HC:SC:PA (8:1:1) on Cu foil | - | 0-2.0V | 20 mA/g | 419 | 361 | 86.1 | 100/93.4% |
| | Glucose (2024)[11] | 1400 °C for 2h in Ar | 1M $NaPF_6$ in diglyme | HC:AB:SA (9:0.5:0.5) on Cu foil | 0.9 | 0.005-2.5V | 20 mA/g<br>50 mA/g | 323.06<br>- | 319.7<br>304.9 | 98.95<br>- | 250/-<br>300/97.9% |
| | Tannin (2024)[12] | 500 °C for 2h then 1400 °C for 2h in Ar | 1M $NaPF_6$ in diglyme | HC:SP:PVDF (8:1:1) on Al foil | - | 0-2.5V | 30 mA/g<br>0.3 A/g<br>1 A/g | 439.8<br>-<br>- | 361<br>309.5<br>169.2 | 82.08<br>-<br>- | -<br>100/-<br>500/94% |
| This work | Thermoplastic elastomer (SBS) | 1 °C/min up to 600 °C followed by 5 °C/min up to 1300 in $N_2$ | 1M $NaPF_6$ in diglyme | HC:AB:SA (8:1:1) on Cu foil | 0.7-1.5 | 0.005-2.5V | 50 mA/g<br>0.5 A/g<br>1 A/g<br>2 A/g | 505<br>403.2<br>342.8<br>138.7 | 391<br>269.7<br>211<br>113.1 | 77.43<br>66.89<br>61.56<br>81.54 | 100/78.99%<br>1000/62.08%<br>1000/51.4%<br>1000/70.73% |

## References


(1) Muruganantham, R.; Hsieh, T.-H.; Lin, C.-H.; Liu, W.-R. Bio-Oil Derived Hierarchical Porous Hard Carbon from Rubber Wood Sawdust via a Template Fabrication Process as Highly Stable Anode for Sodium-Ion Batteries. *Materials Today Energy* **2019**, *14*, 100346. https://doi.org/10.1016/j.mtener.2019.100346.

(2) Pei, L.; Cao, H.; Yang, L.; Liu, P.; Zhao, M.; Xu, B.; Guo, J. Hard Carbon Derived from Waste Tea Biomass as High-Performance Anode Material for Sodium-Ion Batteries. *Ionics* **2020**, *26* (11), 5535–5542. https://doi.org/10.1007/s11581-020-03723-1.

(3) Ou, J.; Zhang, H.; Wang, H.; Lei, Y.; Wu, S. Corn Stalks Derived Hierarchical Porous Carbon as Ultra-Efficient Anode Materials for Sodium-Ion Batteries. *Diamond and Related Materials* **2021**, *120*, 108626. https://doi.org/10.1016/j.diamond.2021.108626.

(4) Hu, H.-Y.; Xiao, Y.; Ling, W.; Wu, Y.-B.; Wang, P.; Tan, S.-J.; Xu, Y.-S.; Guo, Y.-J.; Chen, W.-P.; Tang, R.-R.; Zeng, X.-X.; Yin, Y.-X.; Wu, X.-W. A Stable Biomass-Derived Hard Carbon Anode for High-Performance Sodium-Ion Full Battery. *Energy Technology* **2021**, *9* (1), 2000730. https://doi.org/10.1002/ente.202000730.

(5) Chen, M.; Luo, F.; Liao, Y.; Liu, C.; Xu, D.; Wang, Z.; Liu, Q.; Wang, D.; Ye, Y.; Li, S.; Wang, D.; Zheng, Z. Hard Carbon Derived for Lignin with Robust and Low-Potential Sodium Ion Storage. *Journal of Electroanalytical Chemistry* **2022**, *919*, 116526. https://doi.org/10.1016/j.jelechem.2022.116526.

(6) Lei, Z.-Q.; Xiao, S.-H.; Ran, Z.; Liu, S.-P.; Su, X.-C.; Guo, Y.-J.; Li, W.-X.; Li, Q.; Xu, S.; Yin, Y.-X.; Guo, Y.-G. Circumventing Self-Diffusion Enables High-Rate Hard Carbon Anodes. *Advanced Materials n/a* (n/a), e13193. https://doi.org/10.1002/adma.202513193.

(7) Wu, F.; Zhang, M.; Bai, Y.; Wang, X.; Dong, R.; Wu, C. Lotus Seedpod-Derived Hard Carbon with Hierarchical Porous Structure as Stable Anode for Sodium-Ion Batteries. *ACS Appl. Mater. Interfaces* **2019**, *11* (13), 12554–12561. https://doi.org/10.1021/acsami.9b01419.

(8) Ma, L.; Cao, M.; Zhao, C. song; Huang, S.; Ding, J.; Chen, J.; Zhou, Y. The Novel N-Rich Hard Carbon Nanofiber as High-Performance Electrode Materials for Sodium-Ion Batteries. *Ceramics International* **2021**, *47* (7, Part A), 9118–9124. https://doi.org/10.1016/j.ceramint.2020.12.035.

(9) Wang, C.-C.; Su, W.-L. Understanding Acid Pretreatment of Lotus Leaves to Prepare Hard Carbons as Anodes for Sodium Ion Batteries. *Surface and Coatings Technology* **2021**, *415*, 127125. https://doi.org/10.1016/j.surfcoat.2021.127125.

(10) Xiao, L.; Lu, H.; Fang, Y.; Sushko, M. L.; Cao, Y.; Ai, X.; Yang, H.; Liu, J. Low-Defect and Low-Porosity Hard Carbon with High Coulombic Efficiency and High Capacity for Practical Sodium Ion Battery Anode. *Advanced Energy Materials* **2018**, *8* (20), 1703238. https://doi.org/10.1002/aenm.201703238.

(11) Lu, Z.; Yang, H.; Guo, Y.; Lin, H.; Shan, P.; Wu, S.; He, P.; Yang, Y.; Yang, Q.-H.; Zhou, H. Consummating Ion Desolvation in Hard Carbon Anodes for Reversible Sodium Storage. *Nat Commun* **2024**, *15* (1), 3497. https://doi.org/10.1038/s41467-024-47522-y.

(12) Hu, Q.; Xu, L.; Liu, G.; Hu, J.; Ji, X.; Wu, Y. Understanding the Sodium Storage Behavior of Closed Pores/Carbonyl Groups in Hard Carbon. *ACS Nano* **2024**, *18* (32), 21491–21503. https://doi.org/10.1021/acsnano.4c06281.